Graphene nanomesh: New versatile materials

Article *in* Nanoscale · October 2014

DOI: 10.1039/c4nr04584j · Source: PubMed

6 authors, including:

Jun Yang
Nanjing Tech University
56 PUBLICATIONS **2,814** CITATIONS
SEE PROFILE

Li Laiquan
University of Adelaide
25 PUBLICATIONS **1,956** CITATIONS
SEE PROFILE

Yufei Zhang
Institute of Earth Environment, Chinese Academy of Sciences
84 PUBLICATIONS **2,649** CITATIONS
SEE PROFILE

Wei Huang
University of Hawai'i at Mānoa
1,663 PUBLICATIONS **80,461** CITATIONS
SEE PROFILE

Nanoscale

REVIEW

View Article Online
View Journal | View Issue

Cite this: *Nanoscale*, 2014, **6**, 13301

Graphene nanomesh: new versatile materials

Jun Yang,[a] Mingze Ma,[a] Laiquan Li,[a] Yufei Zhang,[a] Wei Huang*[a,b] and Xiaochen Dong*[a,b]

Received 10th August 2014,
Accepted 15th September 2014

DOI: 10.1039/c4nr04584j

www.rsc.org/nanoscale

Graphene, an atomic-scale honeycomb crystal lattice, is increasingly becoming popular because of its excellent mechanical, electrical, chemical, and physical properties. However, its zero bandgap places restrictions on its applications in field-effect transistors (FETs). Graphene nanomesh (GNM), a new graphene nanostructure with a tunable bandgap, shows more excellent performance. It can be widely applied in electronic or photonic devices such as highly sensitive biosensors, new generation of spintronics and energy materials. These illustrate significant opportunities for the industrial use of GNM, and hence they push nanoscience and nanotechnology one step toward practical applications. This review briefly describes the current status of the design, synthesis, and potential applications of GNM. Finally, the perspectives and challenges of GNM development are presented and some suggestions are made for its further development and exploration.

1. Introduction

Nanostructured materials are increasingly becoming popular due to their high surface-to-volume ratios. For a long time, two-dimensional crystals were considered to be thermodynamically unstable at finite temperatures, and they could not be fabricated until the emergence of graphene. Since its experimental discovery in 2004, the two-dimensional (2D) atomic crystal structure has attracted considerable interest for its potential application as an excellent electrical conductor.[1,2] It can be assembled into 0D fullerenes, 1D nanotubes or 3D graphite. Graphene is a single layer of sp^2-hybridized carbon and has remarkable chemical stability and physical properties such as excellent electrical conductivity, excellent mechanical strength, superior thermal conductivity, and high theoretical surface area (~2630 m^2 g^{-1}).[3] Its potential applications are numerous, including nanoelectronics, nanocomposites, chemical sensors and biosensors, and solar cells.[4] In 2006, Ruoff and co-workers first demonstrated a solution-based process for producing single-layer graphene using graphite oxide (GO) by the Hummers' method.[5,6] After that, several methods have been made available for the mass-production of graphene, *e.g.*, liquid-phase exfoliation of graphite,[7] chemical vapor deposition (CVD),[8] synthesis on silicon carbide (SiC), molecular beam epitaxy, *etc.*[9,10] Among these methods, CVD is one of the most widely used approaches to synthesize large-scale and high quality graphene films based on the possibility of thermal catalytic decomposition of gaseous hydrocarbons on the surface of some metals with the formation of various nanocarbon structures.[11–16] Furthermore, high quality graphene film can be fabricated by the CVD process with organic solvents as carbon source under atmospheric pressure.[17,18] Table 1 describes the different methods employed for the synthesis of graphene film.

Traditional FETs are based on silicon metal–oxide–semiconductor field effect transistors (MOSFET). The miniaturization of MOSFETs has been the key to the progress in integrated circuits. Size scaling has enabled the complexity of integrated circuits to double every 18 months.[19] However, MOSFET scaling is approaching its limits, and in the long run, it will be necessary to introduce new materials to break the Moore's Law to ensure that the FET performance continues to improve. To achieve this goal, a number of FETs, such as GaAs, InP, and silicon n-channel MOSFETs, have been developed.[20] However, these methods require the use of expensive transition-metal elements. Graphene, with high conductivity and 2D structure, is an ideal candidate for the fabrication of FET devices with a single back gate and good electronic properties.[21,22] Compared with traditional electrode materials, graphene-based materials show some novel characteristics.[23] However, devices with the channels made of graphene without sufficient bandgap cannot be switched off at room temperature, and therefore are is not suitable for logic applications. However, the band structure of graphene can be modified by doping, hydrogenation, graphene nanoribbon, graphene nanomesh, or graphene nanoring.[24]

[a]*Jiangsu-Singapore Joint Research Center for Organic/Bio-Electronics & Information Displays and Institute of Advanced Materials (IAM), Nanjing Tech University, 30 South Puzhu Road, Nanjing 211816, China*
[b]*Key Laboratory for Organic Electronics & Information Displays (KLOEID), Nanjing University of Posts and Telecommunications, Nanjing 210046, China. E-mail: iamxcdong@njtech.edu.cn, iamwhuang@njtech.edu.cn*

Table 1 Properties of graphene film obtained by different methods[9]

Method	Crystallite size (μm)	Sample size (mm)	Charge carrier mobility (at ambient temperature) ($cm^2 V^{-1} s^{-1}$)	Applications
Mechanical exfoliation	>1000	>1	$>2 \times 10^5$ and $>10^6$ (at low temperature)	Research
Chemical exfoliation	≤0.1	Infinite as a layer of overlapping flakes	100 (for a layer of overlapping flakes)	Coatings, paint/ink, composites, transparent conductive layers, energy storage, bioapplications
Chemical exfoliation *via* graphene oxide	~100	Infinite as a layer of overlapping flakes	1 (for a layer of overlapping flakes)	Coatings, paint/ink, composites, transparent conductive layers, energy storage, bioapplications
CVD	1000	~1000	10 000	Photonics, nanoelectronics, transparent conductive layers, sensors, bioapplications
SiC	50	100	10 000	High-frequency transistors and other electronic devices

2. Graphene nanoribbons (GNRs)

GNR, as the name suggests, is a thin strip cut along a certain orientation of the graphene plane. There are two types of GNRs: armchair nanoribbons and zigzag nanoribbons (Fig. 1).[25,26] It has been predicted that both of them with narrow widths (below 20 nm) have an open bandgap, and their bandgap is relevant to their widths. The bandgap of GNR can be calculated with the equation: $E_g = 0.8/W$, where E_g is the bandgap and W is the ribbon width in nanometer.[27] Because of their interesting electronic property, GNRs have been demonstrated as a promising candidate material for future post-silicon electronics such as transport materials and FETs.

High-quality GNRs are important in the application of graphene nanoelectronic devices. As a result, there has been significant progress in the fabrication of GNRs, with many new approaches being developed. The main methods are as follows: (1) top-down lithography methods; (2) GNRs from unzipping carbon nanotubes (CNTs); (3) sonochemical method and other chemical method; (4) when top-down meets bottom-up.[28] However, the smallest width produced by lithography approaches is only 15–20 nm, which prevents us from obtaining GNRs with a sufficiently large band gap. Additionally, high quality GNRs with narrow width can be obtained by other methods. For example, Feng's group fabricated GNRs with a width below 10 nm with the top-down and bottom-up method.[29] Huang and co-workers reported a rational approach to fabricate sub-10 nm GNRs using top-down meets bottom-up technology, and the GNRs-FETs have good electric transport performance.[30] In this study, they used pre-synthesized nanowires as etch mask. Compared with conventional lithography, Dai's group showed an approach in making GNRs by unzipping multi-walled carbon nanotubes with plasma etching of nanotubes partly embedded in a polymer film. The GNRs had smooth edges and a narrow width distribution (10–20 nm).[31] Unzipping CNTs with well-defined structures in an array will allow the production of GNRs with controlled widths, edge structures, placement and alignment in a scalable for device integration (Fig. 2).[32] Innovatively, nanowires can be obtained using various chemical approaches with controllable sizes down to 1–2 nm. The widths of the resulting GNRs were mainly determined by mask width (nanowire diameter). But it is difficult to obtain GNRs with smooth edges and controllable widths at high yields with this method. As documented, chemical approaches[33] and self-assembly processes can also produce GNRs of desired shapes and dimensions for fundamental and practical applications.

Owing to the opened bandgap, the GNRs-based FETs present high on–off ratio and excellent electronic properties. For example, the FETs fabricated with a width of 10–15 nm GNRs had an on–off ratio around 10, and the on–off ratio increased sharply when the width shrank down to the sub-10 nm regime.[30] It was reported that the highest room temperature on–off ratio of 10^7 for a GNR-FET was achieved by Dai's group by GNRs synthesized sonochemically with ribbon width in the sub-5 nm regime.[33] Also, it was shown that most experimentally fabricated GNRs-FETs were p-type transistors with charge neutrality point moved to the positive gate region, and

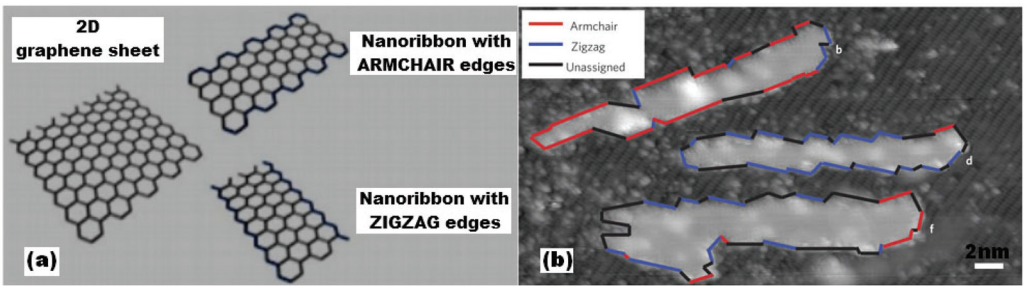

Fig. 1 (a) Zigzag and armchair GNRs;[25] (b) STM topograph of zigzag, armchair and unassigned GNRs with edge symmetries labeled.[26]

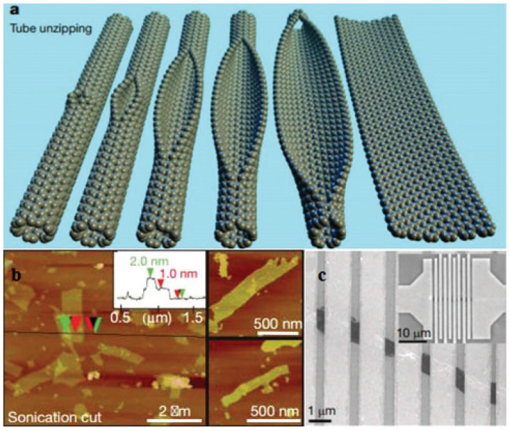

Fig. 2 (a) The gradual unzipping of carbon nanotube to form a nanoribbon. (b) AFM image of partly stacked multiple short fragments of nanoribbons. The height data (inset) indicates the ribbons are generally single layer. The two small images on the right show some other characteristic nanoribbons. (c) SEM image of a multi-terminal device based on multilayer (~10 nm thick) stacked GNRs with platinum electrodes. Inset: larger image of similar device.[32]

with either slightly or heavily suppressed electron transport. It was primarily due to the absorption of charge impurities and oxidation of carbon–carbon bond during the fabrication process.

In addition to the applications in the field of FETs, GNRs also can be used in gas- and bio-sensing,[34,35] memory cell,[36] magnetoresistance[37] and electrochemical lithium storage.[38] The methods for fabricating GNRs are still in development. For instance, Bao's group reported the use of metal salts infused within stretched DNA as catalysts to grow nanoscopic graphitic nanoribbons.[39] The nanoscopic graphitic nanoribbons were micrometre in length, 10 nm in width, and took on the shape of the DNA template. The DNA strand was converted to a graphitic nanoribbon by utilizing CVD. Moreover, Omid *et al.* used GNRs and modified GNRs for selective cancer cell imaging, photothermal therapy, and accelerated differentiation of human neural stem cells.[40–42]

3. Graphene nanomesh

Although GNRs possess opened bandgaps and the GNRs-based FETs present excellent electronic properties, there also exist many problems, such as experimentally observed transport behaviors, edge roughness induced localization effect and coulomb blockade effect, *etc.*[27,43] According to the scaling law, the width of GNR in the sub-10 nm regime is required to achieve sufficiently large bandgap for room temperature transistor operation. For example, a bandgap of 0.67 eV (like Ge) requires a GNR width of 2–3 nm, which is a challenge to fabricate. To ensure GNRs devices come with desired characteristics and their integration into useful circuits precise placement of multiple GNRs into densely organized arrays is required.[44–46] But these methods cannot improve significantly the performance of GNRs. In order to overcome the problems, a new nonzero bandgap derivative of graphene structure, called graphene nanomesh (GNM), was synthesized.[47–53] Basically, GNM comprises singer or few-layer graphene into which a high-density array of nanoscaleholes are punched. This type of nanostructure can also open up a bandgap in large graphene sheets and bestow on it semiconducting performance. The electronic structure of nanomesh is determined not only by the types of edge (zigzag or armchair) but also the amount of edges. Theoretical studies, including the opening of bandgap in the electronic band structure and the dependence of this gap on the GNM porosity and pore lattice symmetry, have been implemented to explore the relationship between GNM structure and electronic properties, mechanical properties and thermal properties.[54–57] Moreover, it was demonstrated that GNM-based transistors could support driving currents nearly 100 times greater than that of individual GNRs devices with a comparable on–off ratio. Therefore, GNM is the most ideal material for transistor channel in terms of delivering a large ON-current. Compared to the basal planes in normal graphene sheets, the nanoscale periodic or quasi-periodic nanoholes within GNM possess more active sites and edges for faster electron transport and higher electrocatalytic activity. It can be concluded that GNM is a new and fascinating nanostructure and will attracted increasing attention.

The bandgap opening in large sheets of graphene has been demonstrated by punching high-density array of periodic nanoholes.[58] Depending on the neck width, the meshing orientation and the shape of holes, a bandgap of higher than 0.5 eV could be achieved.[59,60] In the graphene honeycomb lattice of carbon atoms, the charge transport can be well described by a simple nearest-neighbor tight binding (TB) model. Enormous efforts have been made on theoretical models and calculations on GNM to predict the change in electronic structures due to lattice modification by perforating.[61–63] Fundamental understanding of the gap opening in GNM could be gained using the TB model of the π bond with the nearest-neighbor interaction. William Oswald *et al.* reported that the periodic perturbation induced by periodic nanoscale holes caused a change of GNM between a semimetal and a semiconductor, depending on the variation of lattice vectors.[59] As evidenced by the facts, increasing neck width of a semiconductor GNM reduces the bandgap. Indeed, the GNM-induced bandgap strongly limits the contributions of chiral tunneling and thermionic transmission at the Dirac point and better control of the potential and the thermionic current. One remaining issue that should be considered when designing GNM devices is the atomic edge disorder of the holes. In principle, this disorder can detrimentally affect the output current.

3.1 Methods to fabricate GNM

Because of the special nanostructure of the GNM, the synthesis of large area GNM needs to be demonstrated using the state-of-art techniques to achieve larger device density for realizing its practical applications. Also, it is highly expected that

the prepared GNM can open the graphene bandgap and increase its specific surface area (SSA) and transparency. Up to now, several methods have been developed to fabricate high quality GNM, such as block copolymer lithography, self-assembled monolayers of colloidal microspheres, photocatalytic pattern, and so on. Next, these novel strategies for the fabrication of GNM will be introduced in detail.

3.1.1 Block copolymer lithography. Block copolymer lithography is a novel method for the fabrication of GNM, as shown in Fig. 3. Mechanically peeled graphene flake was used as the starting material, although the approach described here can be readily extended to graphene films obtained through chemical exfoliation or CVD growth. A 10 nm thick silicon oxide (SiO_x) film was first evaporated onto graphene film as the protecting layer and grafting substrate for the subsequent block copolymer nanopattern. The poly(styreneblock-methyl methacrylate) (P(S-*b*-MMA)) block copolymer thin film patterned in cylindrical domains on the surface as etching template and a CHF_3-based reactive-ion etch (RIE) process followed by oxygen plasma etch was used to punch holes into the graphene layer. Following hydrofluoric acid (HF) dip to remove the oxide mask, GNM was obtained, and the free-standing GNM could be lifted off the substrate by etching away the underlying silicon oxide.

To fabricate high quality GNM, top-down lithography combined with block-copolymer spheres have been adopted, but this technique usually suffers from complicated steps, extremely high costs, and contaminations arising from the direct contact mask. For example, block copolymer has a hydrophobic block and a hydrophilic block. The amphiphilic block copolymer molecule could form micelles with a hydrophilic core and a hydrophobic corona in media of low polarity, while aggregates with the opposite composition are exhibited in solvents of high polarity. The BCP can generate ordered structure for etch mask by self-assembly.[51] In this sense, it is expected directly formed GNM can retain its inherent graphene nature.

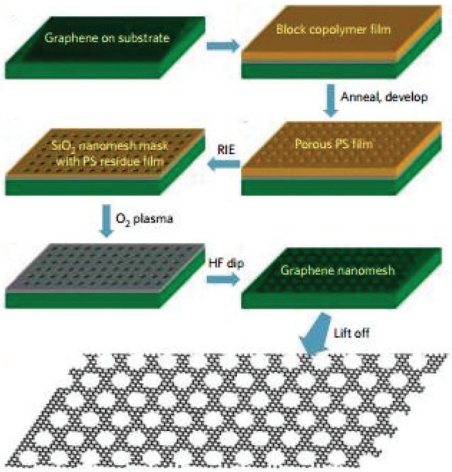

Fig. 3 Schematic of the fabrication of graphene nanomesh.[47]

3.1.2 Nanoparticles local catalytic hydrogenation. The local catalytic approach is another commonly used method to produce GNM, and the process is schematically shown in Fig. 4a. First, the graphene flakes produced by the mechanical cleaving of natural graphite were transferred on SiO_2/Si substrate and annealed at 400 °C in a forming gas (5% hydrogen, 95% ultrahigh purity argon gas) for 5 h to remove absorbents and contamination. Then, a thin Cu film was deposited onto the graphene surface by thermal evaporation in high vacuum. Through controlling the thickness of Cu film and the annealing temperature, various sizes and densities of Cu nanoparticles (NPs) could be formed on the surface of graphene. In the annealing process, with Cu NPs as the catalyst, the graphene under and around the Cu NPs would be dissociated into the Cu NPs and reacted with H_2 to form methane through local catalytic hydrogenation of carbon, and leaving plenty of hole rims around the Cu NPs. After the Cu NPs were removed by Marble's reagent, the graphene regions between the Cu NPs could be reserved and the graphene nanomesh formed. Fig. 4b, c, and d show the SEM images of Cu NPs on the single layer graphene (SLG) by deposition and annealed Cu film with 1, 2, and 4 nm in thickness, respectively. It can be seen that Cu NPs distribute on the surface of SLG uniformly. With the increase of thickness of Cu film from 1 nm to 2 or 4 nm, the average diameter of Cu NPs increased, while the average density of Cu NPs decreased. This result indicates that the size and density of Cu NPs could be easily controlled by the thickness of Cu film. Fig. 4e, f, and g are the SEM images of the resulted graphene nanomesh after the Cu NPs were removed, corresponding to Fig. 4b, c, and d, respectively.[64]

3.1.3 Nanosphere lithography. Nanosphere lithography, or so-called colloidal lithography, is a low-cost and relatively high-throughout technology for patterning nanostructures

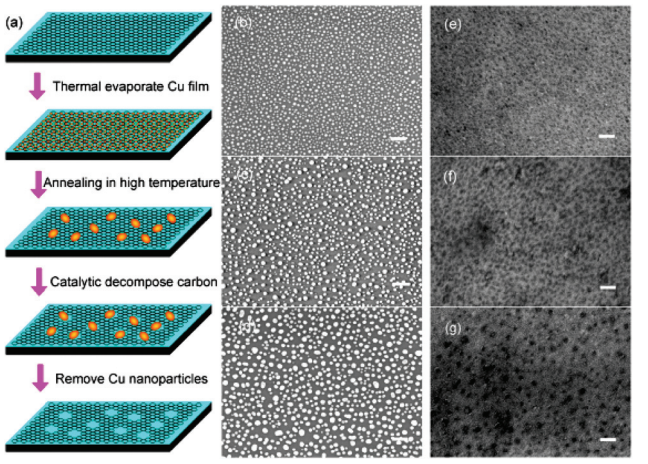

Fig. 4 (a) Schematic diagram for the fabrication of GNM through the local catalytic hydrogenation of carbon in high temperature. (b), (c), and (d) are the SEM images of Cu NPs deposited on single layer graphene with 1, 2, and 4 nm thickness, respectively. (e), (f), and (g) are the SEM images of GNM corresponding to (b), (c), and (d) after the Cu NPs were removed. The scale bar is 200 nm.[64]

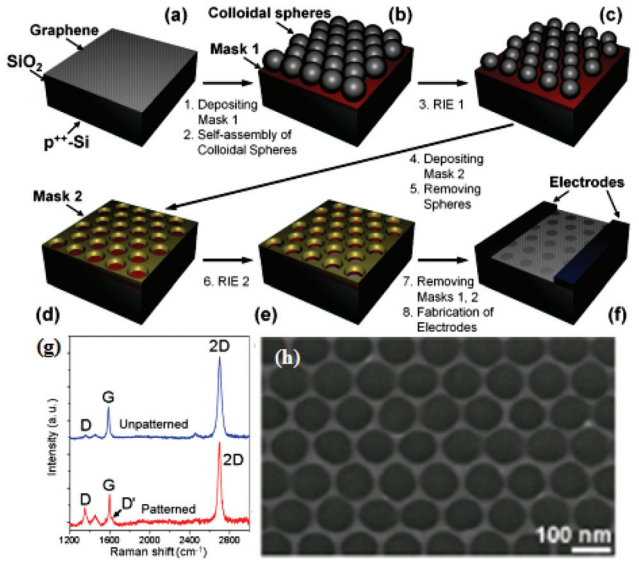

Fig. 5 (a–f) Scheme for the fabrication of GNM. (g) Typical Raman spectra of the unpatterned and patterned graphene areas on the same substrate. (h) SEM image of GNM patterned using 110 nm-sized silica particles.[53]

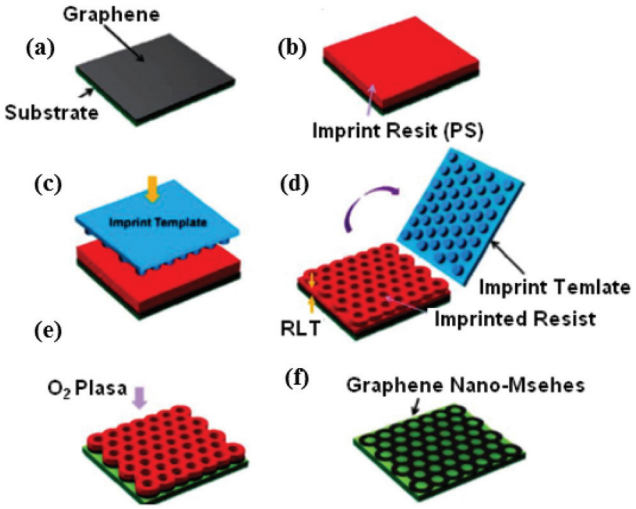

Fig. 6 Schematic fabrication process of GNM by nanoimprint lithography.[65]

without the need for expensive equipment. The key step in nanosphere lithography for producing GNM using colloidal microspheres is by making a periodic porous mask for etching graphene. The fabrication steps for making uniform-sized GNM are presented in detail in Fig. 5. It can be found that this approach is versatile, as different combinations of the mask materials and etching procedures, as well as different colloidal spheres and different approaches for their assembly and removal, can be used. The colloidal spheres were deposited on the substrates by convective self-assembly and removed by ultrasonication in a water bath. The procedure can also be easily adjusted for using other monodisperse spheres, such as polystyrene beads.[53] As shown in Fig. 5g, Raman spectra of the unpatterned areas indicated the synthesized graphene films were mostly monolayers with a less than 1 : 2 G-to-2D intensity ratio, and a symmetrical 2D band was centered at 2690 cm^{-1} with a full width at half-maximum of 35 cm^{-1}. At different areas of the unpatterned graphene, only a tiny D band was observed or not at all, and no D′ band was present. On the contrary, in the patterned areas, both D and D′ bands were clearly observed due to a high percentage of edge atoms in GNM. In GNM with neck width <20 nm, the intensity of the D band was comparable to or higher than that of G band. Fig. 5h shows an SEM image of the GNM obtained by masking etch graphene using 110 nm silica particles. This image demonstrates that narrow (width <20 nm) necks in the GNM are attainable using the described procedure.

Recently, Wang and co-workers have also fabricated GNM on a patterned Cu foil using this technique. The resulting GNM had significantly smoother edges than that of post-growth etched GNM. More importantly, the transistors based on as-grown GNM with neck width of 65–75 nm had a mobility nearly 3-fold higher than those derived from etched GNM with similar neck widths.[50]

3.1.4 Nanoimprint lithography. Nanoimprint lithography is a simple method of fabricating nanometer scale patterns with low cost, high resolution and high throughput. As schematically illustrated in Fig. 6, a graphene nanomesh can be regarded as a quasi-periodic network of multiple GNRs. First, microscopic or larger graphene features are deposited onto a substrate using electrostatic printing of graphene (Fig. 6a), which can incorporate graphene features over large areas and obtain a high yield of monolayers and bilayers. Other methods such as mechanical exfoliation/printing and CVD can also be used here for different purposes. Next, a polymeric resist layer is spin-coated on the top of graphene films (Fig. 6b), and an imprint template bearing hexagonal pillars is used to imprint the hexagonal mesh pattern into the resist layer (Fig. 6c and Fig. 6d). After the imprint process, O_2-based reactive ion etching (RIE) is performed to etch away the underlying graphene and get the nanomesh structures (Fig. 6e). Finally, the resist is removed in a solution, and GNM is formed (Fig. 6f). Such fabrication route is completely based on low-cost, high-throughput lithographic technologies and provides an efficient way to produce ordered graphene nanostructures over large areas.[65]

It is clear that block copolymer lithography, nanoparticles local catalytic hydrogenation, nanosphere lithography, and nanoimprint lithography have different sets of advantages for the fabrication of GNMs and the resulted GNMs have various surface morphologies and electronic performance.

3.1.5 Other methods. Apart from the formerly mentioned GNM fabrication process using lithography technique, there also are some other methods for making GNM. For example, Zhang's group reported idea proof-of-concept using anodic aluminum oxide (AAO) membrane as etching mask to synthesize large area GNM with the help of O_2 plasma etching.[4] As schematically illustrated in Fig. 7, when the thickness of

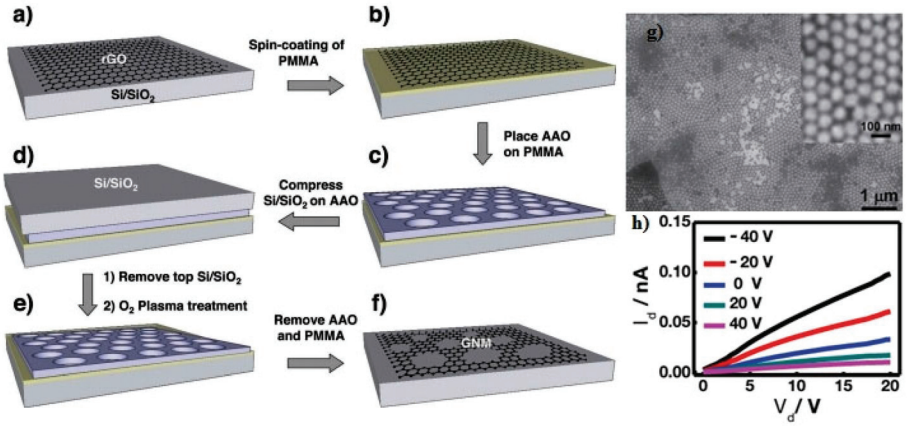

Fig. 7 (a–f) Schematic illustration of GNM fabrication process. (g) SEM image of large-area GNM with pore size of *ca.* 67 nm and neck width of *ca.* 33 nm. (h) I_d–V_d plot of GNM-based FET.[4]

poly(methyl methacrylate) (PMMA) was about 8 nm and etching time about 30–60 s, the porous size of resulted GNM was of uniform distribution. When 8 nm-thick PMMA was used as the adhesion layer and O_2 plasma etching was performed for 30 s, GNM with pore size of *ca.* 67 nm and neck width of *ca.* 33 nm was produced (Fig. 7g). Fig. 7h presents the drain current (I_d) *versus* drain–source voltage (V_d) curves of GNM-based FETs at different gate voltages. Similarly, Park and co-workers fabricated GNM on substrate directly *via* chemical vapor deposition using Au nano-network as the metal catalyst.[20]

However, the presence of PMMA directly contacted on the surface of graphene film complicates the fabrication process in terms of thickness control and the duration of O_2 plasma treatment. Also, the intrinsically isotropic nature of O_2 plasma etching and the relatively long pathway of the oxygen penetrating into the walls of the AAO make it difficult to achieve the desired pattern during etching.

Recently, Fan *et al.* reported an easy method for the synthesis of porous graphene nanosheets (PGNs) with MnO_2 etching the graphene sheets. Moreover, they achieved excellent electrochemical properties in high performance supercapacitors. This approach also offers potentials for cost-effective, environmentally friendly and large-scale production of PGNs (Fig. 8).[66,67]

Akhavan reported a method to prepare GNM by UV-assisted photodegradation using aligned ZnO nanorods as photocatalyst, where the tips of ZnO nanorods were brought into contact with the graphene oxide (GO) sheets and achieved controlled photodegradation of GO. In this work, GNM with a pore size of *ca.* 200 nm was produced. Park's group also reported a method where the graphene meshes were synthesized by CVD on a metal-catalyst layer covered with a self-assembled silica spheres monolayer.[68] In addition, reduced GO nanomesh (rGONM) has also been reported.[69] However, there are still significant challenges for the easy preparation of GNM. So far, GNM is mainly prepared by plasma oxidation of graphene, CVD, or UV-assisted photodegradation of GO sheets

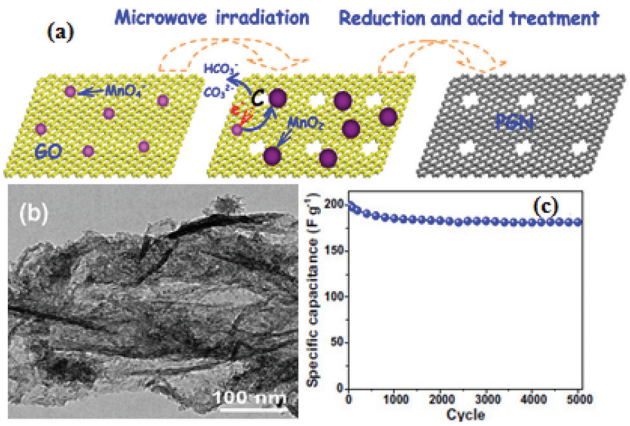

Fig. 8 (a) Illustration of the formation of porous graphene sheet; (b) TEM image of PGNs; (c) cycle stability of the PGN electrode at 100 mV s^{-1} up to 5000 cycles.[67]

with photocatalyst. All the aforementioned approaches have drawbacks, *i.e.*, suffer from low throughput, complexity, high cost, and so on.

3.2 Potential applications of GNM

As mentioned earlier, GNM with opened bandgap and large area is suitable for the fabrication of high performance FETs. Now, most theoretical works on GNM have focused on their electronic[70–75] and mechanical properties.[55,76] In the graphene honeycomb lattice of carbon atoms, the charge transport can be well described by a simple nearest-neighbor tight binding model. Recently, Hung Nguyen *et al.* proposed a model and calculation, which could be used to investigate the exact characteristics of the GNM devices.[77] Also, the operation and electronic performance of GNM-based transistors were investigated systematically.[78] The results indicated that GNM had a greater bandgap because of its more ordered structure, and compared with GNRs, GNM was more suitable for logic applications. More importantly, the GNM-based devices have higher on–off ratio and higher field transport. Potential applications

for GNM include chemical sensing, supercapacitors, DNA sequencing, photothermal therapy, and a new generation of spintronics, among others.[79–81]

3.2.1 Applications in FETs. Owing to the opened bandgap, GNM is suitable for the fabrication of high performance field-effect transistors. In principle, the driving current and on–off ratio of GNM-based transistors are determined by the density and width of the interconnections. The density control was achieved by varying the periodicity of initial polymer mask with polymers precursors of different molecular weight, and the width was controlled by both polymer mask and etching condition. Similar to GNRs device, the GNM-based FET presents typically p-type transistor behavior. But GNM FETs can deliver high current, nearly 100 times greater than individual GNRs devices owing to the large number of conducting channels, and with a comparable on–off ratio that is tunable by varying the neck widths, as shown in Fig. 9. The highest on–off ratio of 100 could be achieved with an average neck width of around 7.0 nm. It should be noted that the requirement to achieve a similar on–off ratio in a bigger GNM device is much more stringent than that in a smaller single GNR device, as each conducting channel needs to be small enough to afford a large on–off ratio. For the first order approximation, GNM can be regarded as a conductive network of multiple GNRs. Therefore, it is expected that the bandgap of GNM is inversely proportional with the average ribbon width (*i.e.*, $E_g \sim \alpha/w$, and α is a coefficient with the unit, nm eV). Furthermore, the on–off ratio of FET is exponentially proportional with the bandgap (*i.e.*, $I_{on}/I_{off} \times \exp(E_g/kT)$, where k is Boltzmann constant and T is the absolute temperature). So the I_{on}/I_{off} value of GNM based FETs on a log scale is expected to be inversely proportional with the average ribbon width, as expressed in eqn (1), where C is a dimensionless constant. To verify this dependence, Fig. 9d shows a semilog plot of the measured I_{on}/I_{off} data (squares) *versus* the inverse of the GNM ribbon-width ($1/w$).

$$I_{on}/I_{off} \propto e^{\alpha/k_B T(l/w)} = Ce^{\alpha/k_B T(l/w)} \quad (1)$$

A more detailed analysis of the bandgap and conduction subbands of GNMs requires a more precise calculation based on a tight-binding model subject to a specific feature edge (zigzag, armchair, or disordered). Such a calculation model is also needed for precisely evaluating the carrier mobility of GNM and other graphene nanostructures. In this work, the carrier mobility of the graphene nanostructures produced by electrostatic printing followed with plasma etching was estimated to be ~1000 cm^2 $(V\ s)^{-1}$ for holes and ~200 cm^2 $(V\ s)^{-1}$ for electrons.[82]

It is important to compare the performance of GNM FETs with those of bulk graphene or GNRs. The on-state conductivity of the nanomesh is approximately 1–2 orders of magnitude lower than that of bulk graphene. The reduced conductance comes from the limited current pathway and the introduction of large quantity of edge defects. The unique structural and electronic characteristics of GNM may also open exciting opportunities in highly sensitive biosensors and new generation of spintronics.[83] In other words, compared with GNRs-based FETs or bulk graphene device, GNM-based FETs have the following advantages: (1) GNM FETs can deliver current nearly 100 times greater than individual GNR devices; (2) on–off ratio can be tunable by varying the neck widths; (3) the on-state conductivity of the nanomesh is approximately 1–2 orders of magnitude lower.

3.2.2 GNM FETs based gas sensors. Besides high electronic performance of transistors, GNM based FETs are very attractive in the sensing field due to their well-defined structure, ease of mass production in high-density array, large contact area, and inherent capability of signal amplification.

As air pollution is becoming more and more serious, the detection standards for gas sensitive devices become more stringent. A lot of materials have been developed to fabricate the sensors, like TiO_2 nanoparticles,[84] tungsten oxide nanowires/porous silicon composite,[85] ZnO nanowires,[86] and so on. Due to its special properties, GNM becomes an ideal material for developing small and compact high performance gas sensors which are cheap and consume little power. For example, Paul's group used CH_4 and ethanol grown GNM films respectively to develop two kinds of FETs, which could be used for gas detection with high sensitivity.[87] In this experiment, GNM FETs were fabricated with Ti (20 nm)/Au (180 nm) as source and drain electrodes. As illustrated in Fig. 10a, gEtOH nanomesh sensor exhibited the best response than a gCH_4 nanomesh sensor, whereas there was no response from their film counterparts. Fig. 10b shows the detection performance of GNM FET sensors to NO_2. The responses over the tested range of 1–10 ppm NO_2 was in the following order: gEtOH nanomesh >gCH_4 nanomesh > gEtOH film > gCH_4 film. Further, the response time, defined as the time required to reach a 90% of the maximum resistance change, for GNM

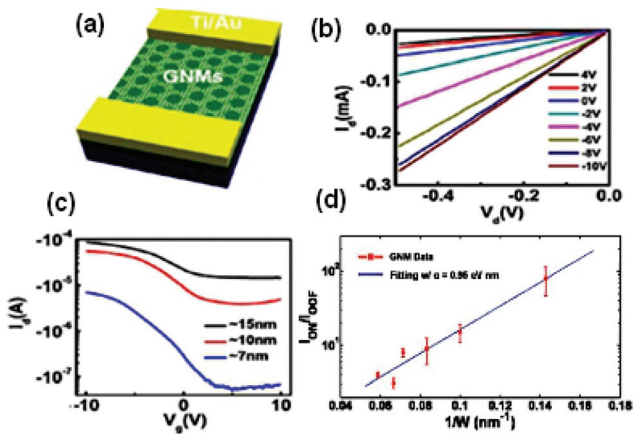

Fig. 9 Electrical properties of GNM based FET. (a) Schematic of GNM-FET. (b) Drain current (I_d) *versus* drain–source voltage (V_d) curves at different gate voltage for GNM FET with channel width ~2 mm and channel length ~1 mm. (c) Transfer characteristics at V_d = –100 mV for GNM FETs with different neck widths.[47] (d) Semilog plot of experimentally measured I_{on}/I_{off} data (squares) as a function of the inverse of GNM ribbon-width ($1/w$).[65]

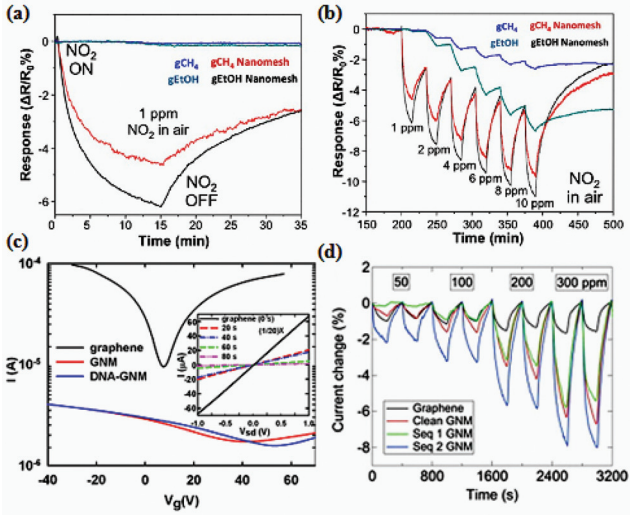

Fig. 10 (a) Current responses of FETs fabricated by gCH_4 and gEtOH grown GNM and their continuous film counterparts to 1 ppm NO_2 in dry air. (b) Dynamic responses of FETs fabricated by gCH_4 and gEtOH grown GNM and their continuous film counterparts exposed to various concentrations of NO_2 in dry air.[77] (c) Current-gate voltage characteristics of different samples with 100 mV source-drain voltage (V_{sd}). Inset: I–V_{sd} curves of GNM and graphene FETs at zero gate voltage. (d) Responses of devices based on graphene, GNM, DNA-GNM based on Seq1, and DNA-GNM based on Seq2 to DMMP.[88]

sensors at 1 ppm NO_2 in dry air was approximately 7 min and decreased to 5 min at 10 ppm.

Recently, Johnson and co-workers found that single-stranded DNA functionalized GNM devices presented high sensitivity, selectivity and reproducibility for gas detection.[88] Here, DNA was bonded onto the surface of GNM *via* π–π stacking interactions between DNA bases and bulk graphene and possibly *via* electrostatic/hydrogen bonding interactions between the primary amines of the bases and oxygen-containing groups at the edges of GNM.[89] Longer etching time caused the electrical resistance to increase from several kilo-ohms to the mega-ohm range (Fig. 10c, inset), consistent with the expected decrease in the width of graphene channels and increased carrier scattering from edge defects. Fig. 10d presents the dynamic responses to increasing concentrations of dimethyl methylphosphonate (DMMP) for FETs based on as-fabricated graphene, GNM, DNA-GNM based on oligomer Seq1, and DNA-GNM based on Seq2. It was observed that as-fabricated graphene devices responded to DMMP at the tested concentrations 50–300 ppm and that the response was essentially saturated at 50 ppm. The GNM response to DMMP was roughly the same as that of CVD graphene for concentrations below 100 ppm (~−2%), but the magnitude of the response increased to ~−8% at 300 ppm. After DNA functionalization, GNM devices showed a sequence-dependent response that reflected the differences in the attraction between DMMP and the two DNA sequences. DNA-GNM devices based on Seq1 showed a smaller vapor response magnitude than unfunctionalized GNM, which was attributed to the suppression of DMMP binding at the GNM edge due to the presence of DNA, while DNA in the bulk region did not provide sufficient affinity for DMMP binding to compensate for the response. In contrast, the responses to DMMP of DNA-GNM devices based on Seq2 were enhanced at all concentrations tested, indicating high affinity between this oligomer and DMMP. Table 2 shows a set of responses for different sorts of devices tested against selected analytes.

It can be seen that DNA functionalization leads to a significant, sequence-dependent increase in the response to all concentrations vapor tests. These attributes make DNA-GNM sensors potentially useful for the detection and classification of vapors consisting of different kinds of compounds over a wide range of concentrations and chemical families. The sequence-dependent behavior in the vapor response data may reflect more complex mechanisms beyond simple electrostatic interactions.[90–92] In addition, the excellent thermal properties of graphene will permit the application of the GNM FETs for high temperature gas sensing. Moreover, operating at higher temperature will improve the sensor response, recovery times and selectivity compared to room temperature operation.[93] It is believed that GNM FETs could potentially be functionalized by other chemical groups and biomaterials for targeted sensing and electronic nose-type applications in either gas or vapor environments.

3.2.3 GNM based FETs biosensors. Owing to the high electron transfer rate, high quenching efficiency, ultra-large planar structure, large surface area, excellent carrier mobility, and good mechanical properties, graphene based FETs have proved to be promising in bio/chemo sensing,[94] such as DNA,[95–100] protein,[101–107] glucose[108–110] and certain kinds of bacteria,[111] and others.[112] The first graphene FET based electrical biosensors were demonstrated by Mohanty *et al.*,[113] who made graphene field-effect transistors from chemically modified graphene, such as reduced graphene oxides or graphene amines. The probe DNAs were anchored onto the surface of graphene, after that complementary DNAs with fluorescent

Table 2 Vapor response for various type devices and analytes[88]

Analyte VOC	Est. conc. (ppm)	Graphene (%)	GNM (%)	GNM-seq1 (%)	GNM-seq2 (%)
DMMP	200	−1.36 ± 0.2	−3.8 ± 0.3	−3.5 ± 0.3	−5.8 ± 0.5
Dinitrotoluene	90	−0.6 ± 0.1	−2.7 ± 0.4	−1.6 ± 0.2	−7.1 ± 0.3
Propionic acid	105	<0.1	<0.1	0.7 ± 0.1	1.3 ± 0.1
Hexanoic acid	8	<0.1	0.5 ± 0.2	0.8 ± 0.1	0.6 ± 0.1
Nonanal	11	−0.2 ± 0.1	−1.3 ± 0.2	−0.3 ± 0.1	−2.7 ± 0.2
Decanal	13	−0.7 ± 0.1	−0.8 ± 0.2	−0.2 ± 0.1	−2.2 ± 0.3

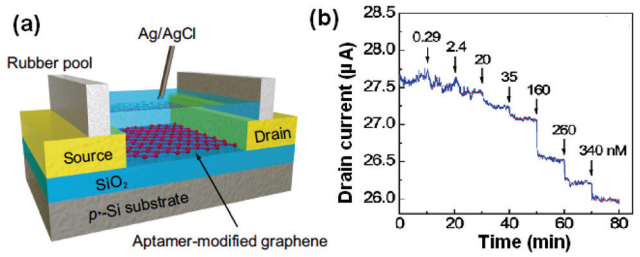

Fig. 11 (a) Schematic illustration of aptamer-modified graphene FETs. (b) Time course of I_d for an aptamer-modified graphene FET. At 10 min intervals, various concentrations of IgE were injected.[114]

activity would hybridize with probe DNAs. The hybridization process would affect the current and the electrical field. By the change of the response current, the target DNAs strand could be investigated easily. The result could be confirmed by the fluorescence. Subsequently, Ohno *et al.* demonstrated a label-free immunosensing based on an aptamer-modified graphene FETs (Fig. 11a). Immunoglobulin E aptamers with an approximate height of 3 nm were successfully immobilized on graphene surface, as confirmed by atomic force microscopy. The aptamer-modified graphene FETs showed a selective electrical detection of immunoglobulin E protein. From the dependence of the drain current variation on the immunoglobulin E concentration, the dissociation constant was estimated to be 47 nM, indicating good affinity (Fig. 11b).[114]

Although, a large number of reports based graphene FETs biosensing have been published, there are almost no reports on GNM FETs for biosensors. Compared with GNRs-based FETs or bulk graphene device, GNM FETs have better performance owing to their high current delivery, high on/off ratio, large edge ratio, and so on. It is believed that GNM can be used to fabricate high performance biosensors in the near future.

3.2.4 Energy storage. Energy and environment are two important considerations in the sustainable development of civilization. The consumption of conventional fossil fuels could be reduced by the use of clean and renewable energies derived from the sun and wind. New materials which can effectively convert and store renewable energies are the key to clean technology. The 2D nanostructures, GNM, have shown some promises in energy storage and conversion. For example, Ning and co-workers used porous MgO layers as templates to synthesize GNM by CVD.[115] The fabrication process, the porous structure, and application of GNM in gas storage are shown in Fig. 12.[116] It indicates that high capacity methane storage (236v(STP)/v) and high selectivity to carbon dioxide adsorption were obtained in the resulting GNM with a high specific surface area (SSA) and a SSA-lossless high bulk density in carbon nanomaterials. Afterwards, Co_3O_4–PGN composite layers were synthesized using GNM as template, which possessed an ultra-high capacity (1543 mA h g^{-1} at 150 mA g^{-1}), excellent rate capability (1075 mA h g^{-1} at 1000 mA g^{-1}) and good cycling stability.[117] In addition, the assembled asymmetric supercapacitor using GNM as a negative electrode and $Ni(OH)_2$–graphene hybrid material as a positive electrode showed great electrochemical performance.[118] Moreover, the nanomeshed structure of GNM could serve as nanoscale vessels to load a huge family of compounds for the synthesis of GNM based composites for the application of high performance Li-ion battery electrode.[119,120] Using ordered structure of GNM, Ren's group was inspired to fabricate highly stretchable and transparent Au nanomesh electrodes that could be applied in foldable photoelectronics and muscle-like transducers.[121] Recently, Qu's group successfully assembled the graphene nanomeshes into the structure-hierarchical foams (GMFs) for the first time, in which the macroporous graphene network was composed of graphene sheets with in-plane nanopores. The N- and S-codoped GMF electrode exhibited excellent electrocatalytic activities for oxygen reduction reaction, which is one of the best among all the graphene-based oxygen reduction catalysts reported previously.[122] These effects indi-

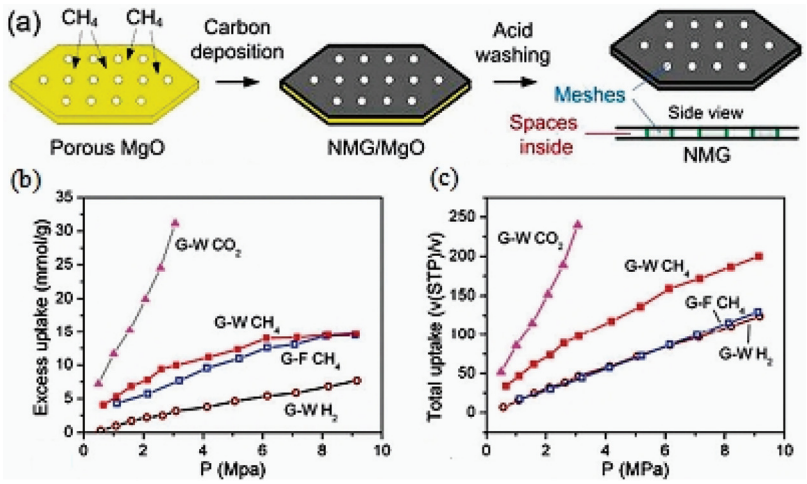

Fig. 12 (a) Illustration of the formation of porous structured nanomesh graphene (NMG). (b) Excess gas uptake of NMG samples. (c) Total volumetric gas uptake of NMG samples.[116]

cated a bandgap might be opened up due to the potential difference induced by the vertical electrical field. This tunable bandgap was confirmed by optical measurement reported by Wang and coworkers in which tunable absorption peak was observed under variable external electric field.[123]

According to the literature, it can be found that GNMs has excellent electronic properties and high performance in FETs compared to GNRs. It is believed that not only can GNM be applied in traditional electronic device configurations, such as field-effect devices,[124] it also provide a platform at a manageable scale for various applications, such as energy storage, environmental remediation, biosensors, catalysis, composite materials, and so on.[125–129] However, besides the cost and the complicated step in obtaining GNM, GNM also has some other problems. For example, the low density of nanoholes and the large distance between the adjoining holes failed to open up the bandgap of graphene for FET operation. Although solution oxidation methods have been recently reported, they could not assemble GNM into multidimensional architectures.[130,131] Thus, potential application fields and fabrication methods for GNM still need to be explored (Fig. 12).

3.2.5 Other potential applications. Recently, graphene based nanoplates attract more and more attention in imaging, targeting and therapy of tumors applications because of its outstanding physicochemical properties. It possesses strong absorption in near-infrared (NIR) and selective uptake in tumors.[132–134] Photothermal therapy is a hyperthermia therapeutic method that usually employs light absorbing agents to kill cancer cells under laser irradiation by heating with high specificity and minimal invasiveness.[135] A large variety of inorganic nanomaterials, such as gold nanostructures,[136] carbon nanomaterials,[137] palladium nanosheets,[138] copper sulfide nanoparticles,[139] and tungsten oxide nanowires[140] have been widely explored. For example, Omid *et al.* proposed GNM to be one of the most promising nanomaterials in both ultralow graphene concentration and laser power photothermal therapy.[69] As shown in Fig. 13, the tumor selectively targeted by rGONM-PEG-Cy7-RGD (reduced graphene oxide nanomesh functionalized by polyethylene glycol (PEG), arginine–glycine–aspartic acid (RGD)-based peptide, and cyanine 7) could be eliminated entirely after ultralow power NIR photothermal therapy. It also proves that GNM has potential applications in ultraefficient cancer diagnosis and therapy with low side effects.

4. Conclusions and outlook

In summary, GNM gives a potential pathway to realizing large scale fabrication of semiconducting materials. Due to its remarkable properties, GNM has become an active research field for future electronic or other applications, such as highly sensitive biosensors, catalysis, composite materials, and so on. Although extensively investigated in laboratory, the fabrication of high performance GNM devices still faces many challenges. First, the quality and availability of "synthetic" graphene will continue to be improved. Second, chemical modification of graphene basal plane or its edges will substantially influence graphene-based devices. The precise control the plane or edges is of great concern. Third, the bandgap in GNM is controlled by the same mechanisms proposed for GNRs, including confinement, edge roughness induced localization and the contribution of Coulomb charging. There are still many issues to further research in a bid to obtain both smooth edges and controlled narrow GNM, which can open a sizable and well-defined bandgap. Fourth, the low density of nanoholes and the large distance between the adjoining holes failed to open up the bandgap of GNM. Additionally, preferential removal of the GNM from the substrate is also vital. However, with the improvement of synthetic routes, the prospect of replacing traditional materials with a low-cost carbon-based coating seems feasible. It is believed that the performance of GNM based devices can be further improved and the new material could be applied in more fields including biosensors, energy storage and photothermal treatment.

Acknowledgements

The project was supported by Jiangsu Provincial Founds for Distinguished Young Scholars (BK20130046), the National Basic Research Program of China (2012CB933300), the NNSF of China (21275076, 61328401), the Key Project of Chinese Ministry of Education (2012058), Program for New Century Excellent Talents in University (NCET-13-0853), Qing Lan Project, Research Fund for the Doctoral Program of Higher Education of China (20123223110008), Synergetic Innovation Center for Organic Electronics and Information Displays, and the Priority Academic Program Development of Jiangsu Higher Education Institutions (PAPD).

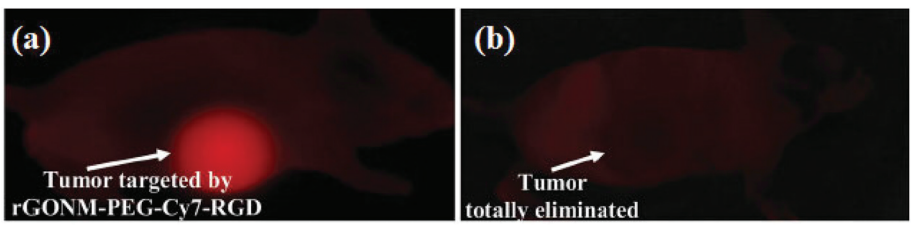

Fig. 13 fluorescence images of Balb/c mice bearing U87MG tumors injected by rGONM-PEG-Cy7-RGD before (a) and after 48 h photothermal treatment (b). The autofluorescence of the mice was removed from the images.[69]

References

1 V. C. Tung, L. Chen, M. J. Allen, J. K. Wassei, K. Nelson, R. B. Kaner and Y. Yang, *Nano Lett.*, 2009, **5**, 1949–1955.
2 A. K. Geim and K. S. Novoselov, *Nat. Mater.*, 2007, **6**, 183–191.
3 N. Xiao, H. Tan, J. Zhu, L. Tan, X. Rui, X. Dong and Q. Yan, *ACS Appl. Mater. Interfaces*, 2013, **5**, 9656–9662.
4 Z. Zeng, X. Huang, Z. Yin, H. Li, Y. Chen, H. Li, Q. Zhang, J. Ma, F. Boey and H. Zhang, *Adv. Mater.*, 2012, **24**, 4138–4142.
5 S. Stankovich, D. A. Dikin, G. H. B. Dommett, K. M. Kohlhaas, E. J. Zimney, E. A. Stach, R. D. Piner, S. T. Nguyen and R. S. Ruoff, *Nature*, 2006, **442**, 282–286.
6 I. Jung, D. A. Dikin, R. D. Piner and R. S. Ruoff, *Nano Lett.*, 2008, **8**, 4283–4287.
7 P. Blake, P. D. Brimicombe, R. R. Nair, T. J. Booth, D. Jiang, F. Schedin, L. A. Ponomarenko, S. V. Morozov, H. F. Gleeson, E. W. Hill, A. K. Geim and K. S. Novoselov, *Nano Lett.*, 2008, **8**, 1704–1708.
8 X. S. Li, W. W. Cai, J. H. An, S. Kim, J. Nah, D. X. Yang, R. Piner, A. Velamakanni, I. Jung, E. Tutuc, S. K. Banerjee, L. Colombo and R. S. Ruoff, *Science*, 2009, **324**, 1312–1314.
9 K. S. Novoselov, V. I. Fal'ko, L. Colombo, P. R. Gellert, M. G. Schwab and K. Kim, *Nature*, 2012, **490**, 192–200.
10 J. Hackley, D. Ali, J. DiPasquale, J. D. Demaree and C. J. K. Richardson, *Appl. Phys. Lett.*, 2009, **95**, 133114.
11 A. V. Eletskii, I. M. Iskandarova, A. A. Knizhnik and D. N. Krasikov, *Phys.-Uspekhi*, 2011, **54**, 227–258.
12 X. C. Dong, P. Wang, W. J. Fang, C. Y. Su, Y. H. Chen, L. J. Li, W. Huang and P. Chen, *Carbon*, 2011, **49**, 3672–3678.
13 S. Bae, H. Kim, Y. Lee, X. Xu, J. Park, Y. Zheng, J. Balakrishnan, T. Lei, H. R. Kim, Y. I. Song, Y. J. Kim, K. S. Kim, B. Ozyilmaz, J. H. Ahn, B. H. Hong and S. Iijima, *Nat. Nanotechnol.*, 2010, **5**, 574–578.
14 H. Sun, Z. Xu and C. Gao, *Adv. Mater.*, 2013, **25**, 2554–2560.
15 J. Lee, P. Lee, H. B. Lee, S. Hong, I. Lee, J. Yeo, S. S. Lee, T. S. Kim, D. Lee and S. H. Ko, *Adv. Funct. Mater.*, 2013, **23**, 4171–4176.
16 Y. Wang, Y. Zheng, X. Xu, E. Dubuisson, Q. Bao, J. Lu and K. P. Loh, *ACS Nano*, 2011, **5**, 9927–9933.
17 X. C. Dong, H. Xu, X. W. Wang, Y. X. Huang, M. Chan-Park, H. Zhang, L. H. Wang, W. Huang and P. Chen, *ACS Nano*, 2012, **6**, 3206–3213.
18 X. Dong, Y. Shi, W. Huang, P. Chen and L. J. Li, *Adv. Mater.*, 2010, **22**, 1649–1653.
19 G. E. Moore, in Tech. Dig. IEEE ISSCC20-23, 2003.
20 F. Schwierz, *Nat. Nanotechnol.*, 2010, **5**, 487–496.
21 K. S. Novoselov, A. K. Geim, S. V. Morozov, D. Jiang, M. I. Katsnelson, I. V. Grigorieva, S. V. Dubonos and A. A. Firsov, *Nature*, 2005, **438**, 197–200.
22 H. B. Heersche, P. J. Herrero, J. B. Oostinga, L. M. K. Vandersypen and A. F. Morpurgo, *Nature*, 2007, **446**, 56–59.
23 Y. Huang, J. Liang and Y. Chen, *Small*, 2012, **8**, 1805–1834.
24 I. Jung, H. Y. Jang and S. Park, *Appl. Phys. Lett.*, 2013, **103**, 023105.
25 X. Jia, J. C. Delgado, M. Terrones, V. Meunier and M. S. Dresselhaus, *Nanoscale*, 2011, **3**, 86–95.
26 K. A. Ritter and J. W. Lyding, *Nat. Mater.*, 2009, **8**, 235–242.
27 X. Li, X. Wang, L. Zhang, S. Lee and H. Dai, *Science*, 2008, **319**, 1229–1232.
28 J. Bai and Y. Huang, *Mater. Sci. Eng. R*, 2010, **70**, 341–353.
29 L. Doessel, L. Gherghel, X. Feng and K. Muellen, *Angew. Chem., Int. Ed.*, 2011, **123**, 2588–2591.
30 J. W. Bai, X. F. Duan and Y. Huang, *Nano Lett.*, 2009, **9**, 2083–2087.
31 L. Jiao, L. Zhang, X. Wang, G. Diankov and H. Dai, *Nature*, 2009, **458**, 877–880.
32 D. V. Kosynkin, A. L. Higginbotham, A. Sinitskii, J. R. Lomeda, A. Dimiev, B. K. Price and J. M. Tour, *Nature*, 2009, **458**, 872–876.
33 A. P. Yu, P. Ramesh, M. E. Itkis, E. Bekyarova and R. C. Haddon, *J. Phys. Chem. C*, 2007, **111**, 7565–7569.
34 F. Schedin, A. K. Geim, S. V. Morozov, E. W. Hill, P. Blake, M. I. Katsnelson and K. S. Novoselov, *Nat. Mater.*, 2007, **6**, 652–655.
35 X. C. Dong, Q. Long, J. Wang, M. Chan-Park, Y. Huang, W. Huang and P. Chen, *Nanoscale*, 2011, **3**, 5156–5160.
36 E. U. Stutzel, M. Burghard, K. Kern, F. Traversi, F. Nichele and R. Sordan, *Small*, 2010, **6**, 2822–2825.
37 J. W. Bai, R. Cheng, F. X. Xiu, L. Liao, M. S. Wang, A. Shailos, K. L. Wang, Y. Huang and X. F. Duan, *Nat. Nanotechnol.*, 2010, **5**, 655–659.
38 T. Bhardwaj, A. Antic, B. Pavan, V. Barone and B. D. Fahlman, *J. Am. Chem. Soc.*, 2010, **132**, 12556–12558.
39 A. Sokolov, F. L. Yap, N. Liu, K. Kim, L. Ci, O. Johnson, H. Wang, M. Vosgueritchian, A. Koh, J. Chen, J. Park and Z. Bao, *Nat. Commun.*, 2013, **4**, 2402.
40 O. Akhavan, E. Ghaderia and H. Emamy, *J. Mater. Chem.*, 2012, **22**, 20626–20633.
41 O. Akhavan, E. Ghaderia and M. Shahsavar, *Carbon*, 2013, **59**, 200–211.
42 O. Akhavan and E. Ghaderia, *J. Mater. Chem. B*, 2013, **1**, 6291–6301.
43 G. Schubert, J. Schleede and H. Fehske, *Phys. Rev. B: Condens. Matter*, 2009, **79**, 235116–235120.
44 O. Akhavan, *ACS Nano*, 2010, **4**, 4174–4180.
45 G. Seol, B. Kumar and J. Guo, *NANO Res.*, 2012, **5**, 164–171.
46 Y. Zhu, X. Li, Q. Cai, Z. Sun, G. Casillas, M. Jose-Yacaman, R. Verduzco and J. M. Tour, *J. Am. Chem. Soc.*, 2012, **134**, 11774–11780.
47 J. Bai, X. Zhong, S. Jiang, Y. Huang and X. Duan, *Nat. Nanotechnol.*, 2010, **5**, 190–194.

48 L. Zhang, S. Diao, Y. Nie, K. Yan, N. Liu, B. Dai, Q. Xie, A. Reina, J. Kong and Z. Liu, *J. Am. Chem. Soc.*, 2011, **133**, 2706–2713.
49 L. Liu, Y. Zhang, W. Wang, C. Gu, X. Bai and E. Wang, *Adv. Mater.*, 2011, **23**, 1246–1251.
50 M. Wang, L. Fu, L. Gan, C. Zhang, M. Rummeli, A. Bachmatiuk, K. Huang, Y. Fang and Z. Liu, *Sci. Rep.*, 2013, **3**, 1238.
51 C. Wang, Y. Mao, D. Wang, Q. Qu, G. Yang and X. Hu, *J. Mater. Chem.*, 2008, **18**, 683–690.
52 M. Kim, N. S. Safron, E. Han, M. S. Arnold and P. Gopalan, *Nano Lett.*, 2010, **10**, 1125–1131.
53 A. Sinitskii and J. M. Tour, *J. Am. Chem. Soc.*, 2010, **132**, 14730–14732.
54 N. C. B. Mostério and A. F. Fonseca, *Phys. Rev. B: Condens. Matter*, 2014, **89**, 195437.
55 C. Carpenter, A. M. Christmann, L. Hu, I. Fampiou, A. R. Muniz, A. Ramasubramaniam and D. Maroudas, *Appl. Phys. Lett.*, 2014, **104**, 141911.
56 R. Martinazzo, S. Casolo and G. F. Tantardini, *Phys. Rev. B: Condens. Matter*, 2010, **81**, 245420.
57 F. P. Ouyang, S. L. Peng, Z. F. Liu and Z. R. Liu, *ACS Nano*, 2011, **5**, 4023–4030.
58 X. Liang, Y. S. Jung, S. Wu, A. Ismach, D. L. Olynick, S. Cabrini and J. Bokor, *Nano Lett.*, 2010, **10**, 2454–2460.
59 W. Oswald and Z. Wu, *Phys. Rev. B: Condens. Matter*, 2012, **85**, 115431.
60 K. Lopata, R. Thorpe, S. Pistinner, X. Duan and D. Neuhauser, *Chem. Phys. Lett.*, 2010, **498**, 334–337.
61 R. Petersen, T. G. Pedersen and A. P. Jauho, *ACS Nano*, 2011, **5**, 523–529.
62 H. Jippo, M. Ohfuchi and C. Kaneta, *Phys. Rev. B: Condens. Matter*, 2011, **84**, 075467.
63 H. Sahin and S. Ciraci, *Phys. Rev. B: Condens. Matter*, 2011, **84**, 035452.
64 J. Liu, H. Cai, X. Yu, K. Zhang, X. Li, J. Li, N. Pan, Q. Shi, Y. Luo and X. Wang, *J. Phys. Chem. C*, 2012, **116**, 15741–15746.
65 X. Liang, Y. S. Jung, S. Wu, A. Ismach, D. L. Olynick, S. Cabrini and J. Bokor, *Nano Lett.*, 2010, **10**, 2454–2460.
66 L. Jiang and Z. Fan, *Nanoscale*, 2014, **6**, 1922–1945.
67 Z. Fan, Q. Zhao, T. Li, J. Yan, Y. Ren, J. Feng and T. Wei, *Carbon*, 2012, **50**, 1699–1712.
68 J. Yi, D. H. Lee, W. W. Lee and W. I. Park, *J. Phys. Chem. Lett.*, 2013, **4**, 2099–2104.
69 O. Akhavan and E. Ghaderi, *Small*, 2013, **9**, 3593–3601.
70 S. Jungthawan, P. Reunchan and S. Limpijumnong, *Carbon*, 2013, **54**, 359–364.
71 R. Sako, N. Hasegawa1, H. Tsuchiya and M. Ogawa, *J. Appl. Phys.*, 2013, **113**, 143702.
72 H. Sahin and S. Ciraci, *Phys. Rev. B: Condens. Matter*, 2011, **84**, 035452.
73 R. Petersen, T. G. Pedersen and A. P. Jauho, *ACS Nano*, 2011, **5**, 523–529.
74 I. I. Naumov and A. M. Bratkovsky, *Phys. Rev. B: Condens. Matter*, 2012, **85**, 201414(R).
75 N. O. Weiss, H. Zhou, L. Liao, Y. Liu, S. Jiang, Y. Huang and X. Duan, *Adv. Mater.*, 2012, **24**, 5782–5825.
76 Y. J. Sun, F. Ma and X. W. Xu, *Integrated Ferroelectrics*, 2011, **128**, 118–124.
77 V. H. Nguyen, F. Mazzamuto, J. Saint-Martin, A. Bournel and P. Dollfus, *Nanotechnology*, 2012, **23**, 065201.
78 S. Berrada, V. H. Nguyen, D. Querlioz, J. Saint-Martin, A. Alarcon, C. Chassat, A. Bournel and P. Dollfus, *Appl. Phys. Lett.*, 2013, **103**, 183509.
79 P. T. Xu, Y. J. Xiang, W. K. Sai, Z. Zhen and S. P. Wen, *Chin. Sci. Bull.*, 2012, **57**, 2948–2955.
80 A. Girdhara, C. Sathe, K. Schulten and J. P. Leburton, *Proc. Natl. Acad. Sci. USA*, 2013, **110**, 16748–16753.
81 J. Liu, Y. Xue, M. Zhang and L. Dai, *MRS Bull.*, 2012, **37**, 1265–1272.
82 X. Liang, A. S. P. Chang, Y. Zhang, B. D. Harteneck, H. Choo, D. L. Olynick and S. Cabrini, *Nano Lett.*, 2009, **9**, 467–472.
83 S. Park, D. H. Lee, J. Xu, B. Kim, S. W. Hong, U. Jeong, T. Xu and T. P. Russell, *Science*, 2009, **323**, 1030–1033.
84 J. Esmaeilzadeh, S. Ghashghaie, P. Sowti-khiabani, A. Hosseinmardi, E. Marzbanrad, B. Raissi and C. Zamani, *J. Eur. Ceram. Soc.*, 2014, **34**, 1201–1208.
85 S. Ma, M. Hu, P. Zeng, M. Li, W. Yan and Y. Qin, *Sens. Actuators B*, 2014, **192**, 341–349.
86 H. Nguyen, C. T. Quy, N. D. Hoa, N. T. Lamc, N. V. Duy, V. V. Quang and N. V. Hieu, *Sens. Actuators B*, 2014, **193**, 888–894.
87 R. K. Paul, S. Badhulika, N. M. Saucedo and A. Mulchandani, *Anal. Chem.*, 2012, **84**, 8171–8178.
88 A. Esfandiar, N. J. Kybert, E. N. Dattoli, G. H. Han, M. B. Lerner, O. Akhavan, A. Irajizad and A. T. C. Johnson, *Appl. Phys. Lett.*, 2013, **103**, 183110.
89 T. Premkumar and K. E. Geckeler, *Prog. Polym. Sci.*, 2012, **37**, 515–644.
90 Y. Dan, Y. Lu, N. J. Kybert, Z. Luo and A. T. C. Johnson, *Nano lett.*, 2009, **9**, 427–432.
91 Y. Lu, B. R. Goldsmith, N. J. Kybert and A. T. Charlie Johnson, *Appl. Phys. Lett.*, 2010, **97**, 083107.
92 M. B. Lerner, J. M. Resczenski, A. Amin, R. R. Johnson, J. I. Goldsmith and A. T. C. Johnson, *J. Am. Chem. Soc.*, 2012, **134**, 14318–14321.
93 J. D. Fowler, M. J. Allen, V. C. Tung, Y. Yang, R. B. Kaner and B. H. Weiller, *ACS Nano*, 2009, **3**, 301–306.
94 Y. X. Liu, X. C. Dong and P. Chen, *Chem. Soc. Rev.*, 2012, **41**, 2283–2307.
95 X. C. Dong, W. Huang and P. Chen, *Nanoscale Res. Lett.*, 2011, **6**, 60.
96 Z. Yin, Q. He, X. Huang, J. Zhang, S. Wu, P. Chen, G. Lu, P. Chen, Q. Zhang, Q. Yan and H. Zhang, *Nanoscale*, 2012, **4**, 293–297.
97 S. R. Guo, J. Lin, M. Penchev, E. Yengel, M. Ghazinejad, C. S. Ozkan and M. Ozkan, *J. Nanosci. Nanotechnol.*, 2011, **11**, 5258–5263.
98 L. Zhu, L. Luo and Z. Wang, *Biosens. Bioelectron.*, 2012, **35**, 507–511.

99 B. Cai, S. Wang, L. Huang, Y. Ning, Z. Zhang and G. J. Zhang, *ACS Nano*, 2014, **8**, 2632–2638.
100 X. Dong, Y. Shi, W. Huang, P. Chen and L. J. Li, *Adv. Mater.*, 2010, **22**, 1649–1653.
101 X. Liu, L. Shi, X. Hua, Y. Huang, S. Su, Q. Fan, L. Wang and W. Huang, *ACS Appl. Mater. Interfaces*, 2014, **6**, 3406–3412.
102 S. Mao, G. Lu, K. Yu, Z. Bo and J. Chen, *Adv. Mater.*, 2010, **22**, 3521–3526.
103 K. Mao, D. Wu, Y. Li, H. Ma, Z. Ni, H. Yu, C. Luo, Q. Wei and B. Du, *Anal. Biochem.*, 2012, **422**, 22–27.
104 D. J. Kim, I. Y. Sohn, J. H. Jung, Q. J. Yoon, N. E. Lee and J. S. Park, *Biosens. Bioelectron.*, 2013, **41**, 621–626.
105 Q. He, S. Wu, S. Gao, X. Cao, Z. Yin, H. Li, P. Chen and H. Zhang, *ACS Nano*, 2011, **5**, 5038–5044.
106 J. L. Her, T. M. Pan, W. Y. Lin, K. S. Wang and L. J. Li, *Sens. Actuators., B*, 2013, **182**, 396–400.
107 B. Zhan, C. Liu, H. Shi, C. Li, L. Wang, W. Huang and X. Dong, *Appl. Phys. Lett.*, 2014, **104**, 243704.
108 Y. Huang, X. Dong, Y. Shi, C. M. Li, L. J. Li and P. Chen, *Nanoscale*, 2010, **2**, 1485–1488.
109 T. Kavitha, A. I. Gopalan, K. P. Lee and S.-Y. Park, *Carbon*, 2012, **50**, 2994–3000.
110 X. Wang, X. Dong, Y. Wen, C. Li, Q. Xiong and P. Chen, *Chem. Commun.*, 2012, **48**, 6490–6492.
111 Q. He, H. G. Sudibya, Z. Yin, S. Wu, H. Li, F. Boey, W. Huang, P. Chen and H. Zhang, *ACS Nano*, 2010, **4**, 3201–3208.
112 S. J. Park, O. S. Kwon, S. H. Lee, H. S. Song, T. H. Park and J. Jang, *Nano Lett.*, 2012, **12**, 5082–5090.
113 N. Mohanty and V. Berry, *Nano Lett.*, 2008, **8**, 4469–4476.
114 Y. Ohno, K. Maehashi and K. Matsumoto, *J. Am. Chem. Soc.*, 2010, **132**, 18012–18013.
115 G. Ning, Z. Fan, G. Wang, J. Gao, W. Qian and F. Wei, *Chem. Commun.*, 2011, **47**, 5976–5978.
116 G. Ning, C. Xu, L. Mu, G. Chen, G. Wang, J. Gao, Z. Fan, W. Qian and F. Wei, *Chem. Commun.*, 2012, **48**, 6815–6817.
117 X. Zhu, G. Ning, X. Ma, Z. Fan, C. Xu, J. Gao, C. Xu and F. Wei, *J. Mater. Chem. A*, 2013, **1**, 14023–14030.
118 J. Yan, Z. Fan, W. Sun, G. Ning, T. Wei, Q. Zhang, R. Zhang, L. Zhi and F. Wei, *Adv. Funct. Mater.*, 2012, **22**, 2632–2641.
119 Z. Fan, J. Yan, G. Ning, T. Wei, L. Zhi and F. Wei, *Carbon*, 2013, **60**, 558–561.
120 X. Zhu, X. Song, X. Ma and G. Ning, *ACS Appl. Mater. Interfaces*, 2014, **6**, 7189–7197.
121 C. F. Guo, T. Sun, Q. Liu, Z. Suo and Z. Ren, *Nat. Commun.*, 2014, **5**, 3121, DOI: 10.1038/ncomms4121.
122 Y. Zhao, C. Hu, L. Song, L. Wang, G. Shi, L. Dai and L. Qu, *Energy Environ. Sci.*, 2014, **7**, 1913–1918.
123 Y. Zhang, T. T. Tang, C. Girit, Z. Hao, M. C. Martin, A. Zettl, M. F. Crommie, Y. R. Shen and F. Wang, *Nature*, 2009, **459**, 820–823.
124 F. Bonaccorso, Z. Sun, T. Hasan and A. C. Ferrari, *Nat. Photonics*, 2010, **4**, 611–622.
125 Y. Q. Sun, Q. O. Wu and G. Q. Shi, *Energy Environ. Sci.*, 2011, **4**, 1113–1132.
126 I. Jung, H. Y. Jang, J. Moonb and S. Park, *Nanoscale*, 2014, **6**, 6482–6486.
127 J. Zhang, F. Zhao, Z. Zhang, N. Chen and L. Qu, *Nanoscale*, 2013, **5**, 3112–3126.
128 C. Li and G. Q. Shi, *Nanoscale*, 2012, **4**, 5549–5563.
129 S. Nardecchia, D. Carriazo, M. L. Ferrer, M. C. Gutierrez and F. del Monte, *Chem. Soc. Rev.*, 2013, **42**, 794–830.
130 Y. Lin, K. A. Watson, J. W. Kim, D. W. Baggett, D. C. Working and J. W. Connell, *Nanoscale*, 2013, **5**, 7814–7824.
131 S. Liang, M. Yi, Z. Shen, L. Liu, X. Zhang and S. Ma, *RSC Adv.*, 2014, **4**, 16127–16131.
132 K. Yang, S. Zhang, G. Zhang, X. Sun, S. T. Lee and Z. Liu, *Nano Lett.*, 2010, **10**, 3318–3323.
133 H. Y. Mao, S. Laurent, W. Chen, O. Akhavan, M. Imani and M. Mahmoudi, *Chem. Rev.*, 2013, **113**, 3407–3424.
134 A. Nourmohammadi, R. Rahighi, O. Akhavan and A. Moshfegh, *J. Alloys Compd.*, 2014, **612**, 380–385.
135 E. Boisselier and D. Astruc, *Chem. Soc. Rev.*, 2009, **38**, 1759–1782.
136 Z. Zhang, L. Wang, J. Wang, X. Jiang, X. Li, Z. Hu, Y. Ji, X. Wu and C. Chen, *Adv. Mater.*, 2012, **24**, 1418–1423.
137 X. Liu, H. Tao, K. Yang, S. Zhang, S. T. Lee and Z. Liu, *Biomaterials*, 2011, **32**, 144–151.
138 X. Huang, S. Tang, X. Mu, Y. Dai, G. Chen, Z. Zhou, F. Ruan, Z. Yang and N. Zheng, *Nat. Nanotechnol.*, 2010, **6**, 28–32.
139 Q. Tian, M. Tang, Y. Sun, R. Zou, Z. Chen, M. Zhu, S. Yang, J. Wang, J. Wang and J. Hu, *Adv. Mater.*, 2011, **23**, 3542–3547.
140 Z. Chen, Q. Wang, H. Wang, L. Zhang, G. Song, L. Song, J. Hu, H. Wang, J. Liu, M. Zhu and D. Zhao, *Adv. Mater.*, 2013, **25**, 2095–2100.